Desalination and Water Treatment
www.deswater.com

doi: 10.5004/dwt.2021.27544

233 (2021) 62–69
September

Petroleum refinery wastewater treatment using rGo-biochar composite – parametric studies and neural network modeling

Rajamohan Natarajan[a,*], Fatma Al Shibli[a], Rajasimman Manivasagan[b]

[a]*Chemical Engineering Section, Faculty of Engineering, Sohar University, Sohar, PC:311, Sultanate of Oman, emails: rnatarajan@su.edu.om (R. Natarajan), fatmaalshibl21@gmail.com (F. Al Shibli)*
[b]*Department of Chemical Engineering, Annamalai University, India, email: simms@rediffmail.com*

Received 10 April 2021; Accepted 21 June 2021

ABSTRACT

Petroleum refinery wastewater treatment is a serious challenge due to the presence of complex organics and recalcitrant pollutants. In this research study, reduced graphene oxide – biochar composite material was synthesized and applied to treat the refinery wastewater. The effect of operating parameters namely, initial effluent pH (4.0–10.0), composite dosage (0.25–5.0 g/L), initial effluent COD (340–1,360 mg/L), agitation speed (0–400 rpm) and temperature (30°C–40°C) were studied. At pH 8.0, composite dose 4.0 g/L, shaking speed 300 rpm, temperature 35°C, and the initial COD 1,360 mg/L, rGO removed 82% of the effluent COD. The COD reduction efficiency increased, and COD uptake decreased with an increase in composite dose. The kinetic modeling was carried out using three kinetic models namely, pseudo-second-order, power function, and Elovich model. The pseudo-second-order model fitted well with the experimental data ($R^2 > 0.970$) and the root mean square error was evaluated. The pseudo-second-order kinetic constant was evaluated and found to be 0.7×10^{-4} g/(mg min) with the actual refinery effluent at 35°C. The COD uptake achieved in this study is comparable with other studies and confirmed the suitability of the composite for refinery effluent treatment. ANN modeling was used to model the data and predicted with good levels of agreement.

Keywords: Refinery; Graphene oxide; Uptake; Kinetics

1. Introduction

Petroleum refining involves a complex combination of physical and chemical processes aimed at cracking the crude into desired fractions with diversified properties. The petroleum crude processing is a water-intensive process with a high steam requirement in the process stream and utility requirements [1]. The water consumption in the refineries is reported to be in the ratio of 10–19 units of volume for every 100 volumes of crude [1]. The water utilized often leads to the generation of huge volumes of wastewater with daily average of 100,000 barrels operating capacities with most of the leading petroleum refineries. The water released are from different sections of the refinery and contains pollutants including oil, unrecovered petroleum fractions, metals, phenol, inorganic miscellaneous constituents, and many other hydrocarbon traces [2]. The petroleum refinery effluent is unique in terms of diversified contaminants that present a unique challenge to degrade all the pollutants in a single or series of operations [3]. The hydrocarbon contaminants like benzene are reported to be carcinogenic and their complete removal is mandatory by the environmental pollution monitoring and regulatory bodies [4,5]. Treatment of petroleum refinery waste was attempted by conventional methods which are physical and chemical techniques such as coagulation, precipitation, ion exchange, oxidation, adsorption, etc., and modern techniques like membrane

* Corresponding author.

separation, photocatalytic and advanced oxidation methods [6,7]. Biological methods present an alternative to the physico-chemical methods and involve the use of aerobic and anaerobic microorganisms. To combine the advantageous features of different methods, hybrid methods, also called combination methods, are investigated to degrade the refinery wastewater [8]. Most of these conventional methods are less favored due to the lower efficiency of treatment, higher carbon footprint, production of secondary pollutants, and incompatibility with low pollutant concentrations in the effluent [9]. Adsorption, a surface property-based method, is always considered an effective technique to treat oil-based impurities which are resistant to chemical and biological oxidation methods [10]. Conventional adsorbents like activated carbon, clay, fly ash, and charcoal are extensively employed and found unsuitable due to excessive cost and reduced efficiency [11,12]. Carbon-based nano-adsorbents are the new class of materials found to be more suitable for pollution control applications due to their excellent surface properties [13–15]. Enhanced surface area for monolayer graphene was reported as 2.630 m^2/kg of the material. Modified forms of carbon-based nano-adsorbents have gained high importance due to their high selectivity and target specificity. Closely packed carbon atoms in a honeycomb structure with a single sp^2 hybridization pattern were found to promote the uptake capacity of the graphene-based adsorbents [16,17]. Application of graphene and its derivatives for removal of dye molecules have produced successful results and the favorable properties responsible for the same were identified as porosity, surface area, and active sites for dye molecule interaction [17–20]. The presence of negatively charged oxygen groups in the graphene oxide and its derivatives are found to enhance the adsorption capacity and efficiency. Reduced graphene oxide (rGO) is proposed by several researchers for the effective removal of single or multiple ionic groups in solution [21,22]. Biochar, an eco-friendly adsorbent synthesized from natural biomass, has gained attention for environmental pollution control applications [23]. There is no study reported on the use of rGO for the treatment of refinery wastewater and the novelty of this study is related to the synthesis of hybrid nanocomposite using rGO. In this experimental study, a novel hybrid nanocomposite was synthesized using rGO and biochar and employed for the treatment of petroleum refinery wastewater. The parametric experiments were conducted in order to identify the optimal conditions namely effluent pH, COD, speed of agitation, and operating temperature. The mechanism of COD reduction by the rGO-DPB composite was verified using the pseudo-second-order, power function, and Elovich models. The thermodynamic parameters are evaluated to understand the nature of sorption.

2. Materials and methods

2.1. Preparation of composite

The date palm tree, *Phoenix dactylifera*, was used as a source for biochar synthesis [24]. Date palm tree barks were extensively washed to remove dirt, dried in sun for 48 h and reduced to the desired size (<2 cm) using a sieve shaker. The dried plant biomass was crushed into a fine powder and sieved through 0.6 mm screen. The fine powder was pyrolyzed at 600°C for 3 h in an oxygen-lean environment and the biochar produced, date palm biochar (DPB) was stored for further use in airtight plastic containers. Reduced graphene oxide was synthesized from graphite powder using sulfuric acid, potassium permanganate, and sodium nitrate mixture. The oxidized form was exfoliated to separate the fine sheets and further reduced using hydrazine hydrate to produce reduced graphene oxide (rGO) [25]. The rGO – DPB composite was produced by dispersing 4 g of rGO and 8 g of DPB in 1 L of deionized water and sonicated for 30 min (Branson, USA). The sonicated product was filtered using a CA membrane (Sigma Aldrich, EU) and dried at 80°C in an oven (Memmert, USA).

2.2. Batch experiments on COD reduction

The untreated petroleum refinery wastewater was analyzed to determine the physicochemical characteristics namely, pH 8.00, chemical oxygen demand (COD) 1,360 mg/L, total solids 1,326 mg/L, and oil and grease 560 mg/L. Under batch operating conditions, the refinery effluent was treated under pre-determined values of process variables. The effluent pH was chosen as the first parameter to be varied in the range of 4.0–10.0, while other parameters are fixed. The influence of rGO-DPB dose was examined in the range 0.25–5.0 g/L, at optimal pH identified through the first experiment. The ability of the sorbent to handle a wide range of effluent concentrations was studied in the COD range of 340–1,360 mg/L. Temperature effects were monitored by conducting studies at 30°C, 35°C, and 40°C in a thermostatic water bath shaker. All the experiments (except the effect of temperature studies). The treated water samples were analyzed for residual COD after filtering the sample [26]. The COD adsorbed during the contact time was estimated using % COD reduction, given in Eq. (1).

$$\%\text{COD reduction} = \left(\frac{C_0 - C_e}{C_0}\right) \times 100 \tag{1}$$

COD uptake, a measure of removal per unit weight of composite, is defined in Eq. (2).

$$q_e = \frac{V\left(C_0 - C_e\right)}{m} \tag{2}$$

where q_e is the mg of COD removed/g of adsorbent, C_0 and C_e (mg L^{-1}) are the initial and equilibrium COD values, respectively, V is the volume of the effluent (L) and m is the mass of rGO-DPB composite (g). The average of the three readings are reported in the calculations.

2.3. ANN Modelling

Artificial neural network modeling is a useful tool and applied widely for the prediction of process performance in environmental applications. The generalized regression neural network (GRNN) is one of the feed-forward neural network techniques on non-linear regression theory and comprises four layers namely the input, pattern, summation,

and output layers. The architecture of GRNN is shown in Fig. 1. The first three layers consist of fully connected neurons and selective connections to the summative layer. Radial basis function was used for computation of activation and has unity as its maximum when input is zero. Data fitting is usually experimented by using a smaller spread for close-fitting. The output units usually decide the summation units and unsupervised training patterns are employed in GRNN.

3. Results and discussion

3.1. Characteristics of the sorbent

The surface morphology of the synthesized sorbent was examined using the scanning electron microscopic imaging (100x), as shown in Fig. 2. The sorbent material was found to have a multilayered surface with internal cracks and suit adsorption of contaminants from the wastewater. The surface patterns suitable for sorption are clearly visible in the SEM image (Jeol, USA). The rGO-DPB composite was found to have folded edges and resulted in better diffusion between the layers and enhanced adsorption.

3.2. Effect of pH

The industrial effluent is always susceptible to have pH variations due to the change in the composition of the discharged compounds. In this set of experiments, the effluent pH was varied using buffer addition (either 0.1 M HCl or NaOH). The COD reduction efficiency increased from 60% (at pH 4.0) to 82% (at pH 8.0) as presented in Fig. 3. The attainment of lower efficiency at acidic pH could be related to the competition of the excess hydrogen ions with the negatively charged ionic pollutants in the effluent to be adsorbed on the rGO-DPB composite surface. When the pH was increased above 8.0 in the alkaline range, the COD reduction efficiency decreased, and this phenomenon was related to the precipitation effect under hyper alkaline conditions. In addition, the rGO-DPB composite could have negatively charged unconverted oxygen functional groups. Under acidic conditions, these groups undergo neutralization. Removal of malachite green dye using rGO reported similar observations [27]. Lower uptake capacities using rGO for removal of tetracycline were reported at lower pH values [10].

3.3. Effect of composite dosage

Adsorption of solute ions by the sorbent surface is dependent on the surface-active sites. The surface area made available, represented by composite dosage, is identified as a key design variable for the scale up of this batch process. The effect of rGO-DPB composite dose was studied from 0.25 to 5.0 g/L of the effluent, under optimal conditions of pH. Fig. 4 confirmed the directly proportional relationship between dose and the percentage COD reduction. The maximum COD reduction of 82% was reported at a dosage of 4 g/L. The increase in COD reduction percentage was found to be linear in the dosage range of 0.25–4 g/L and no change was observed in the dosage range of 4.0–5.0 g/L. At higher dosages, the availability

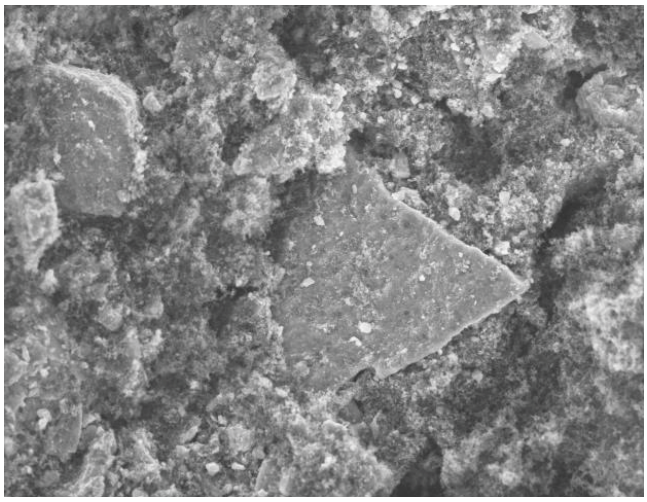

Fig. 2. SEM micrographs of rGO-DPB composite.

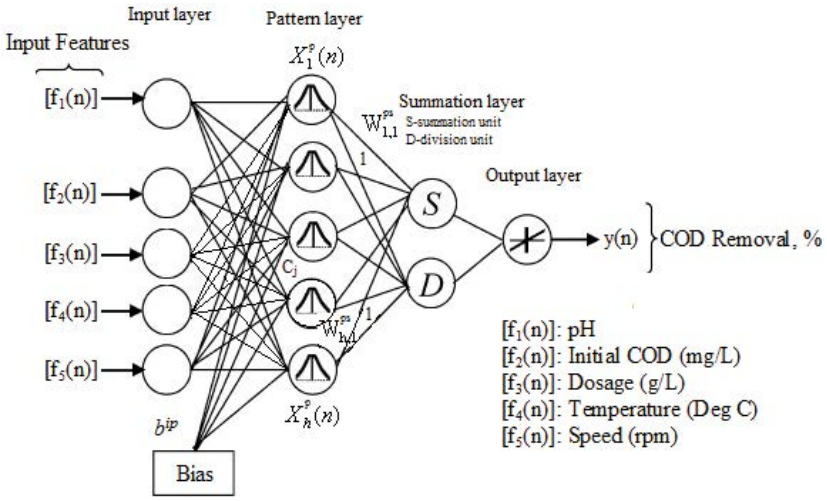

Fig. 1. Structure of GRNN.

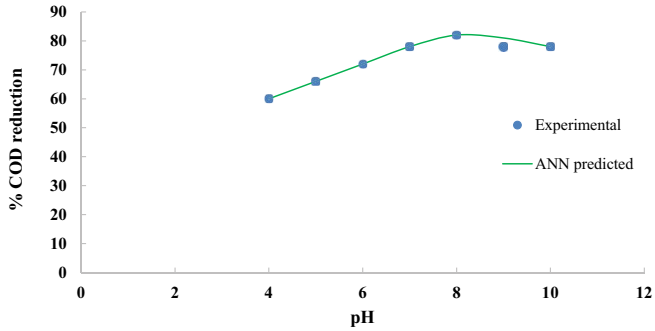

Fig. 3. Influence of initial effluent pH on COD reduction (COD_0 = 1,360 mg/L; w = 4 g/L; T = 35°C; speed = 300 rpm).

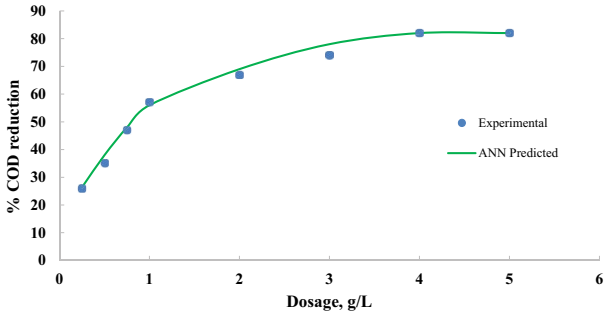

Fig. 4. Influence of rGO-DPB composite dose on the COD reduction and uptake (COD_0 = 1,360 mg/L; pH = 8; T = 35°C; speed = 300 rpm).

of free surface area and the number of active sites were higher, and this contributed to better COD reduction percentages. Higher adsorbent quantities often result in incomplete saturation leading to reduced sorption. The influence of adsorbent dosage on COD uptake was found to be inverse with lower uptakes achieved at higher dosages and the COD uptake decreased from 357 to 170.8 mg/g with an increase of composite dosage from 0.25 to 5 g/L. Non-uniform contact and negative interactions between excessive sites adjacent to each other at high adsorbent concentrations were found to reduce the COD uptakes. The empirical equation relating the COD uptake (q_e) and composite dosage (m) is given by Eq. (3):

$$q_e = 405.71e^{-0.114m} \quad (3)$$

Adsorption studies on removal of COD from tannery wastewater reported a similar effect of dosage on percentage removal efficiency [28]. A study using modified activated sludge for refinery effluent reported an uptake of 153.846 mg/g was reported at a dosage of 8 g/L [29].

3.4. Effect of contact time and initial effluent concentration

Treatment of refinery effluent using rGO-DPB composite was conducted for an equilibrium time of 360 min and the rate of COD reduction was evaluated under fixed intervals of time. The effluent was tested at diluted concentrations with an average initial COD values of 340, 680, 1,020 and 1,360 mg/L at optimal pH identified from the first set of experiments. The time versus COD reduction plot was given in Fig. 5 confirmed higher percentages of COD reduction achieved with effluents having lesser initial COD and due to the vacant surface active sites, the rate of adsorption was found to be faster during the early contact phase. Ion exchange, micro-precipitation, and complex formation were identified as the possible reasons for the better sorption during the initial period. The COD reduction achieved was found to be maximum (96%) with a diluted effluent having initial COD 340 mg/L. The COD reduction percentages were observed with an increase in effluent COD values. With effluents having higher COD values of 1,020 and 1,360 mg/L, the COD reduction percentages decreased to 86% and 82% at an equilibrium time of 300 min. With high concentration effluents, the ratio between the sorbate

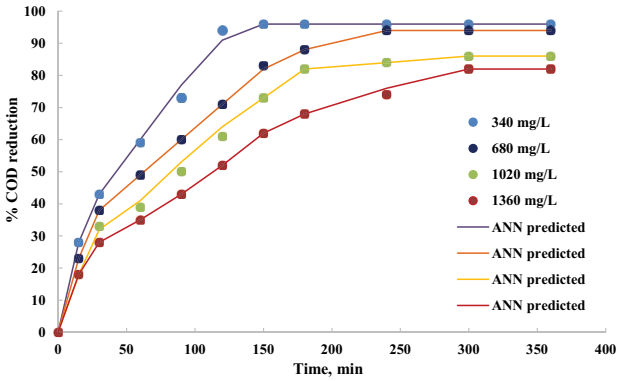

Fig. 5. Influence of effluent concentration on the COD reduction (pH = 8; T = 35°C; w = 4 g/L).

pollutant molecules and sorption sites is higher and could hinder adsorption of more molecules or ions. The performance of the adsorbent was comparable with the other study reported on petroleum refinery effluent treatment [6]. Treatment of refinery effluent using modified activated sludge reported 84% COD reduction when the initial COD was 3,400 mg/L [29].

3.5. Effect of speed of agitation

Adsorption is a surface phenomenon-based separation technique and the degree of mixing is reported to promote better contact between the sorbate molecule and sorbent surface. The contact between the surface sites of the adsorbent and the sorbate ions is better at higher speeds. In this set of experiments, the samples were contacted with rGO-DPB composite under different agitation speeds namely 0, 100, 200, 300 and 400 rpm. The conditions optimized from the previous set of experiments were employed in terms of pH and rGO-DPB dosage. Results obtained at different speeds were presented in Fig. 6 and the COD uptake increased from 8% to 82% when the shaking speed increased from 0 to 300 rpm. Mass transfer rate through the film and reduced boundary layer thickness were found to be responsible for the attainment of higher COD uptakes at higher speed.

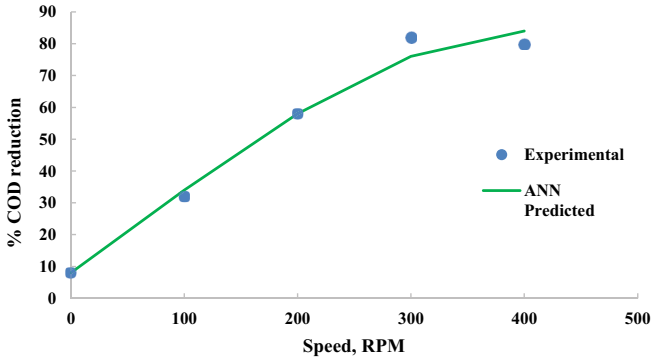

Fig. 6. Effect of agitation speed on the COD reduction (pH = 8; T = 35°C; w = 4 g/L).

At the maximum speed of 400 rpm, the COD decreased to 137.2 mg/g, which could be due to excessive shear force or lack of homogeneity in the sorbate-sorbent system.

3.6. Effect of operating temperature

Temperature influences the sorption rate either by activation of the surface and excitation of the solute. The effect of temperature on the COD reduction percentage by the rGO-DPB composite was studied in the range of 30°C–40°C. From Fig. 7, it was inferred that the COD reduction percentages decreased with an increase in temperature. The maximum COD reduction percentage obtained was 87% at an operating temperature of 30°C. Better sorption at higher temperatures confirmed the nature of the process as chemical sorption and the sorption by rGO-DPB composite was found to be exothermic. Removal of malachite green by rGO followed exothermic sorption with similar observations and the uptakes decreased when the temperature increased from 30°C to 50°C [26].

3.7. COD reduction prediction using generalized regression neural network

In the GRNN model, the spread factor is determined using a stochastic approach. For COD reduction, the network was run several times to evaluate the best spread factor. In both testing and training, the validation was made in terms of the resultant spread factor for COD reduction that produced minimal MAPE error and GRNN network performance is shown in Fig. 8. The neural network model employed consisted of input layer embedded with 5 neurons and output layer with 1 (COD reduction) neuron. The GRNN is selected as the network type with spread factor for COD reduction for training and testing. The network is implemented using the MATLAB neural network toolbox. Fig. 8 shows the spread factor versus the performance predicted by GRNN for COD reduction. The performance of GRNN increases for the spread factor values from 0.01 to 1 is shown in Fig. 8. Maximum performance 99.99% occurs at the spread value 0.05. After that, the performance of GRNN is gradually reducing for COD reduction. A comparison between experimental and ANN models were made and it is depicted in Figs. 2–7. In all the figures, the ANN predicts

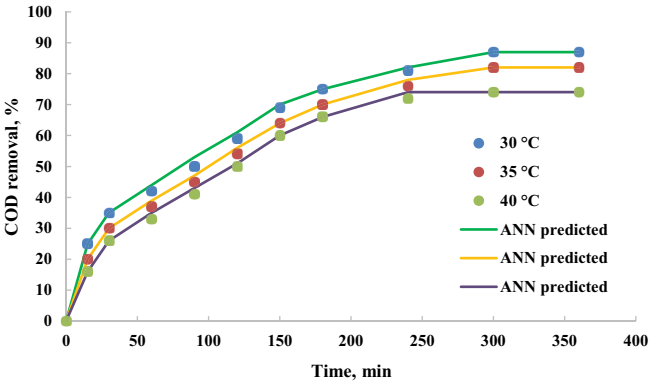

Fig. 7. Effect of operating temperature on the COD reduction (pH = 8; speed = 300 rpm; w = 4 g/L).

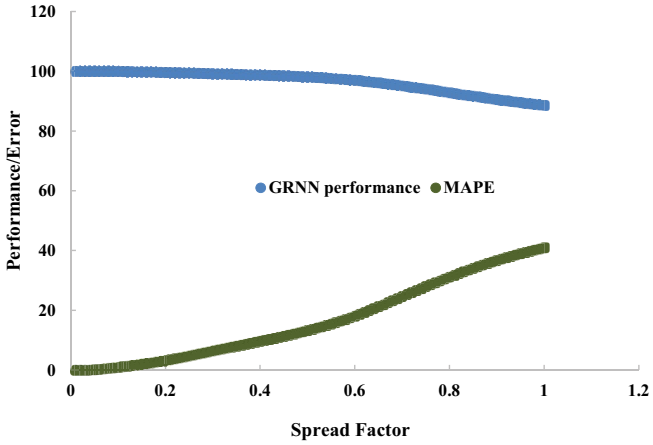

Fig. 8. GRNN performance against spread factor.

the data well and it closely follows experimental data. The correlation coefficient for the ANN predicted data and experimental data was found to be 0.9354. The ANN has the advantages of predicting the data outside the design space which is more useful as far as the application is concerned in a large scale. Thus, the ANN-based model is more flexible and allows the addition of unused experimental data to build a fresh trustworthy model [30]. The results of this study show that the ANN model has better accuracy in predicting the COD reduction.

3.8. Kinetic model

The COD reduction kinetic studies are aimed to understand the mechanism and required to design a continuous separator for large-scale applications. The pseudo-second-order equation, a widely employed model, is fitted to the experimental data [31]. The linearized form of this model [Eq. (4)] was applied to analyze the adsorption kinetics of COD reduction.

$$\frac{t}{q} = \frac{1}{k_1 q_1^2} + \frac{1}{q_1} t \tag{4}$$

where q_1 (mg g^{-1}) is the maximum adsorption capacity and q (mg g^{-1}) is the COD adsorbed at time, t,

and k_1 (g (mg min)$^{-1}$) is the equilibrium rate constant for the pseudo-second-order adsorption.

The power function model, represented in Eq. (5), is a modified form of Freundlich equation.

$$q = k_p t^n \tag{5}$$

where k_p and n (usually positive and <1) are model constants. Eq. (5) is empirical except when n = 1/2, where it is a parabolic diffusion equation [32].

Elovich model proposed an exponentially inverse relationship between the quantity of solute and adsorption rate and is represented by Eq. (6) in its linearized form [33].

$$q = \frac{1}{b}\ln(ab) + \frac{1}{b}\ln t \tag{6}$$

where a denotes the initial adsorption rate (mg/(g min)) and b denotes the desorption constant (g/mg). The three kinetic models were fitted to the experimental data and represented in Figs. 9, 10 and 11. The pseudo-second-order model (Fig. 9) was found to be the best fitting model with comparatively higher values of R^2 (>0.975). Based on this observation, the rate-determining step was identified as surface adsorption which involved chemisorption. The slopes and intercepts from the linear plots were used to evaluate the model constants for pseudo-second order and Elovich models and tabulated in Table 3. The best-fit equation parameters found with the power function model were used to evaluate the model constants. The pseudo-second-model rate constant (k_1) was found to vary from 6.7 × 10^{-4} to 0.7 × 10^{-4} g/(mg min) when the effluent COD increased from 360 to 1,320 mg/L. The error function analysis is presented in Table 1.

3.9. Thermodynamic studies

To evaluate the effect of temperature on the adsorption process of BY28 and BR46 onto GO, the thermodynamic parameters such as a change in free energy (ΔGO), enthalpy (ΔHO), and entropy (ΔSO) were determined using following Eqs. (7) and (8) [34].

$$\ln\left(\frac{q_e}{C_e}\right) = \frac{\Delta S}{R} - \frac{\Delta H}{RT} \tag{7}$$

$$\Delta G = \Delta H - T\Delta S \tag{8}$$

The linear plot between $\ln(q_e/C_e)$ and $(1/T)$ is shown in Fig. 12. From the slope and intercept, the thermodynamic parameters namely enthalpy change (ΔH) and entropy change (ΔS) are evaluated as −67.71 and 0.222 kJ/mol K, respectively. The free energy of adsorption (ΔG) was evaluated using Eq. (8) and found to be −136.42 kJ/mol. These values are in the typical range of chemisorption [35]. The negative values of enthalpy change denote the exothermic nature of the process and positive value of entropy confirms the feasibility of the sorption.

4. Conclusion

The utilization of a novel composite made from rGO and date palm biochar was successfully employed for the treatment of refinery effluent. The favorable surface properties with the synthesized adsorbent were studied using the SEM imaging. The effect of pH on COD reduction efficiency proved that the optimal pH was the neutral range with lower adsorption at acidic pH. The increase in composite dosage produced higher COD reduction percentages and lower uptakes. The COD uptake achieved at an optimal dose of 4 g/L is 170.8 mg/g. The removal of COD by rGO-DPB composite was found to be exothermic and the nature of sorption was confirmed by the pseudo-second-order as chemisorption. The pseudo-second-order model constant, q_1, was found to be 153.846 mg/g

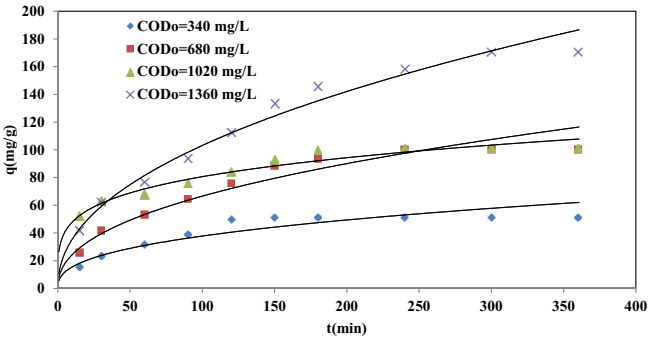

Fig. 10. Power function model plot for the COD reduction using rGO-DPB composite.

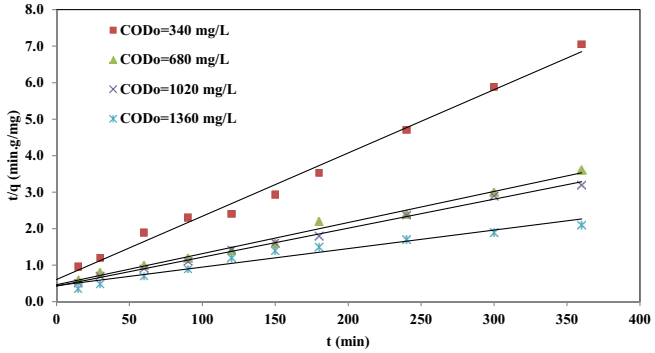

Fig. 9. Pseudo-second-order model plot for the COD reduction using rGO-DPB composite.

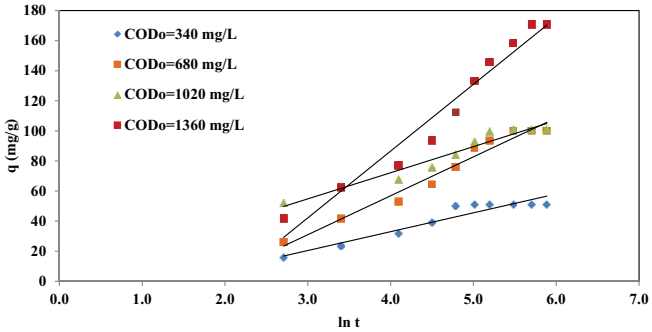

Fig. 11. Elovich model plot for the COD reduction using rGO-DPB composite.

Table 1
Kinetic constants for refinery effluent treatment

Kinetic model	Initial effluent COD (mg/L)			
COD_0 (mg/L)	340	680	1020	1360
Pseudo-second-order				
k_1 (g/(mg min) × 10^4	6.7	3.7	3.3	0.7
q_1 (mg/g)	41.322	78.740	109.890	153.846
R^2	0.990	0.991	0.995	0.979
RMSE	5.65	5.60	5.10	7.6
Adj. R^2	0.9821	0.9812	0.9854	0.9687
MAE	3.26	3.25	3.11	3.88
Power function				
k_p (mg g/min$^{1/2}$)	4.553	6.4001	28.407	8.7685
N	0.387	0.436	0.227	0.462
R^2	0.902	0.964	0.961	0.976
RMSE	14.85	8.69	8.56	8.23
MAE	6.23	4.55	4.52	4.42
Elovich	0.8854	0.9400	0.9399	09425
b (g/mg)	0.112	0.054	0.058	17.349
a (mg/g min)	2.287	3.050	20.343	4.084
R^2	0.912	0.970	0.948	0.958
RMSE	12.51	7.90	10.62	11.33
Adj. R^2	0.8905	0.9522	0.9244	0.9321
MAE	5.98	3.96	4.79	5.22

RMSE – Root mean square error; MAE – Mean absolute error

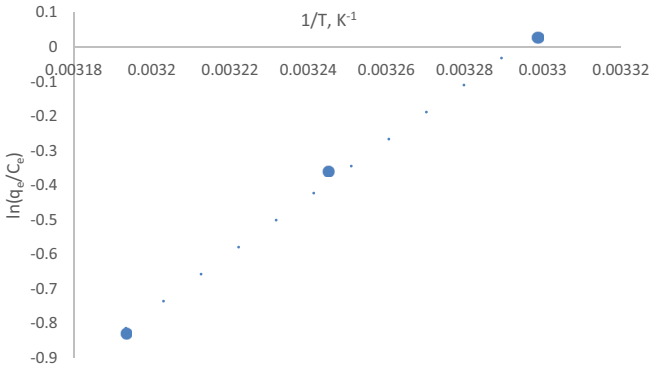

Fig. 12. Thermodynamic plot.

at an initial effluent COD of 1,320 mg/L. Power function and Elovich model constants were evaluated at different effluent concentrations. GRNN modeling predicted the sorption data well with lesser data. The feasibility of the sorption process was verified using Gibbs energy.

References

[1] P. Sun, A. Elgowainy, M. Wang, J. Han, R.J. Henderson, Estimation of US refinery water consumption and allocation to refinery products, Fuel, 221 (2018) 542–557.
[2] R. Singh, D.V. Naik, R.K. Dutta, P.K. Kanaujia, Biochars for the removal of naphthenic acids from water: a prospective approach towards remediation of petroleum refinery wastewater, J. Clean. Prod., J. Cleaner Prod., 266 (2020) 121986, doi: 10.1016/j.jclepro.2020.121986.
[3] J.H. Gary, G.E. Handwerk, M.J. Kaiser, Petroleum Refining: Technology and Economics, CRC Press, USA, 2007.
[4] F. Qaderi, A.H. Sayahzadeh, M. Azizi, Efficiency optimization of petroleum wastewater treatment by using of serial moving bed biofilm reactors, J. Cleaner Prod., 192 (2018) 665–677.
[5] B. Singh, P. Kumar, Pre-treatment of petroleum refinery wastewater by coagulation and flocculation using mixed coagulant: optimization of process parameters using response surface methodology (RSM), J. Water Process Eng., 36 (2020) 101317, doi: 10.1016/j.jwpe.2020.101317.
[6] M.H. El-Naas, R. Surkatti, S. Al-Zuhair, Petroleum refinery wastewater treatment: a pilot scale study, J. Water Process Eng., 14 (2016) 71–76.
[7] Y. Jiang, A. Khan, H. Huang, Y. Tian, X. Yu, Q. Xu, L. Mou, J. Lv, P. Zhang, P. Liu, L. Deng, Using nano-attapulgite clay compounded hydrophilic urethane foams (AT/HUFs) as biofilm support enhances oil-refinery wastewater treatment in a biofilm membrane bioreactor, Sci. Total Environ., 646 (2019) 606–617.
[8] B.H. Diya'uddeen, W.M. Daud, A.A Aziz, Treatment technologies for petroleum refinery effluents: a review, Process Saf. Environ. Prot., 89 (2011) 95–105.
[9] C. Chen, X. Yan, Y. Xu, B.A. Yoza, X. Wang, Y. Kou, H. Ye, Q. Wang, Q.X. Li, Activated petroleum waste sludge biochar for efficient catalytic ozonation of refinery wastewater, Sci. Total Environ., 651 (2019) 2631–2640.
[10] A.M. Huízar-Félix, C. Aguilar-Flores, A. Martínez-de-la Cruz, J.M. Barandiarán, S. Sepúlveda-Guzmán, R. Cruz-Silva, Removal of tetracycline pollutants by adsorption and magnetic separation using reduced graphene oxide decorated with α-Fe_2O_3 nanoparticles, J. Nanomater., 9 (2019) 313, doi: 10.3390/nano9030313.
[11] M. Elazzouzi, K. Haboubi, M.S. Elyoubi, Electrocoagulation flocculation as a low-cost process for pollutants removal from urban wastewater, Chem. Eng. Res. Des., 117 (2017) 614–626.
[12] M.L. Davis, S.J. Masten, Principles of Environmental Engineering, McGraw-Hill Education, USA, 2013.
[13] N. Van Quy, N.D. Hoa, M. An, Y. Cho, D. Kim, A high-performance triode-type carbon nanotube field emitter for mass production, Nanotechnology, 18 (2007) 345201.
[14] K. Lü, G. Zhao, X. Wang, A brief review of graphene-based material synthesis and its application in environmental pollution management, Sci. Bull., 57 (2012) 1223–1234.
[15] N. Pandey, S.K. Shukla, N.B. Singh, Water purification by polymer nanocomposites: an overview, J. Nanostruct. Polym. Nanocomposites, 3 (2017) 47–66.
[16] Y. Liu, J. Ma, T. Wu, X. Wang, G. Huang, Y. Liu, H. Qiu, Y. Li, W. Wang, J. Gao, Cost-effective reduced graphene oxide-coated polyurethane sponge as a highly efficient and reusable oil-absorbent, ACS Appl. Mater. Interfaces, 5 (2013) 10018–10026.
[17] L. Das, P. Das, A. Bhowal, C. Bhattachariee, Synthesis of hybrid hydrogel nano-polymer composite using graphene oxide, chitosan and PVA and its application in wastewater treatment, Environ. Technol. Innovation, 18 (2020) 100664, doi: 10.1016/j.eti.2020.100664.
[18] D. Baragaño, R. Forján, L. Welte, J.L.R. Gallego, Nanoremediation of As and metals polluted soils by means of graphene oxide nanoparticles, Sci. Rep., 10 (2020) 1–10.
[19] W. Yu, L. Sisi, Y. Haiyan, L. Jie, Progress in the functional modification of graphene/graphene oxide: a review, RSC Adv., 10 (2020) 15328–15345.
[20] E. Çalışkan Salihi, J. Wang, G. Kabacaoğlu, S. Kırkulak, L. Šiller, Graphene oxide as a new generation adsorbent for the removal of antibiotics from waters, Sep. Sci. Technol., 56 (2021) 453–461.
[21] C.P.M. de Oliveira, M.M. Viana, M.C.S. Amaral, Coupling photocatalytic degradation using a green TiO_2 catalyst to membrane bioreactor for petroleum refinery wastewater reclamation, J. Water Process Eng., 34 (2020) 101093, doi: 10.1016/j.jwpe.2019.101093.
[22] C.Z. Zhang, B. Chen, Y. Bai, J. Xie, A new functionalized reduced graphene oxide adsorbent for removing heavy metal ions in

water via coordination and ion exchange, Sep. Sci. Technol., 53 (2018) 2896–2905.
[23] S.M. Shaheen, N.K. Niazi, N.E. Hassan, I. Bibi, H. Wang, D.C. Tsang, Y.S. Ok, N. Bolan, J. Rinklebe, Wood-based biochar for the removal of potentially toxic elements in water and wastewater: a critical review, Int. Mater. Rev., 64 (2019) 216–247.
[24] R.A. Al-Alawi, J.H. Al-Mashiqri, J.S. Al-Nadabi, B.I. Al-Shihi, Y. Baqi, Date palm tree (*Phoenix dactylifera* L.): natural products and therapeutic options, Front. Plant Sci., 8 (2017) 845, doi: 10.3389/fpls.2017.00845.
[25] Y. Hou, S. Lv, L. Liu, X. Liu, High-quality preparation of graphene oxide via the Hummers' method: understanding the roles of the intercalator, oxidant, and graphite particle size. Ceram. Int., 46 (2020) 2392–2402.
[26] R.B. Baird, Standard Methods for the Examination of Water and Wastewater, 23rd ed., Water Environment Federation, American Public Health Association, American Water Works Association, USA, 2017.
[27] K. Gupta, O.P. Khatri, Reduced graphene oxide as an effective adsorbent for removal of malachite green dye: plausible adsorption pathways, J. Colloid Interface Sci., 501 (2017) 11–21.
[28] R. Natarajan, R. Manivasagan, Treatment of tannery effluent by passive uptake-parametric studies and kinetic modeling, Environ. Sci. Pollut., 25 (2018) 5071–5075.
[29] N. Rajamohan, A. Al-Sadi, K.P. Ramachandran, Treatment of refinery waste water using modified sludge – effect of process parameters, sorbent characterization and kinetic studies, Desal. Water Treat., 57 (2016) 19741–19749.
[30] V.R. Moreira, Y.A. Lebron, L.V. de Souza Santos, Predicting the biosorption capacity of copper by dried *Chlorella pyrenoidosa* through response surface methodology and artificial neural network models, Chem. Eng. J. Adv. 4 (2020) 100041, doi: 10.1016/j.ceja.2020.100041.
[31] Y.S. Ho, G. McKay, Pseudo-second order model for sorption processes, Process Biochem., 34 (1999) 451–465.
[32] A.A. Inyinbor, F.A. Adekola, G.A. Olatunji, Kinetics, isotherms and thermodynamic modeling of liquid phase adsorption of Rhodamine B dye onto *Raphia hookerie* fruit epicarp, Water Resour. Ind., 15 (2016) 14–27.
[33] F.C. Wu, R.L Tseng, R.S. Juang, Characteristics of Elovich equation used for the analysis of adsorption kinetics in dye-chitosan systems, Chem. Eng. J., 150 (2009) 366–373.
[34] S. Karagoz, T. Tay, S. Ucar, M. Erdem, Activated carbons from waste biomass by sulfuric acid activation and their use on methylene blue adsorption, Bioresour. Technol., 99 (2008) 6214–6222.
[35] G. Crini, P.M. Badot, Sorption Processes and Pollution. Conventional and Non-Conventional Sorbents for Pollutant Removal from Wastewaters, Presses universitaires de Franche-Comté, France, 2010.